BNL-100819-2013-IR

Partial Return Yoke for MICE

Holger Witte, Stephen Plate

May 3, 2013

Collider-Accelerator Department / Magnet Division

Brookhaven National Laboratory

U.S. Department of Energy
Office of Science

DISCLAIMER

Partial Return Yoke for MICE

Holger Witte*, Stephen Plate[1]

[1]Brookhaven National Laboratory, P.O. Box 5000, Upton, NY, 11973, USA

May 3, 2013

The international Muon Ionization Cooling Experiment (MICE) is a large scale experiment which is presently assembled at the Rutherford Appleton Laboratory in Didcot, UK. The purpose of MICE is to demonstrate the concept of ionization cooling experimentally. Ionization cooling is an important accelerator concept which will be essential for future HEP experiments such as a potential Muon Collider or a Neutrino Factory. The MICE experiment will house up to 18 superconducting solenoids, all of which produce a substantial amount of magnetic flux.

Recently it was realized that this magnetic flux leads to a considerable stray magnetic field in the MICE hall. This is a concern as technical equipment in the MICE hall may may be compromised by this.

In July 2012 a concept called 'partial return yoke' was presented to the MICE community, which reduces the stray field in the MICE hall to a safe level. This report summarizes the general concept, engineering considerations and the expected shielding performance.

*hwitte@bnl.gov

1. Introduction

MICE, which is an acronym for Muon Ionization Cooling Experiment, is a large-scale international high energy physics experiment which is aiming to demonstrate the concept of ionization cooling experimentally. Muon cooling is an essential concept for future accelerators such as a Muon Collider and the Neutrino Factory, as ionization cooling is the only known technology fast enough to reduce the emittance of a muon beam. Successful muon cooling has an impact on the accelerator performance as well as the cost.

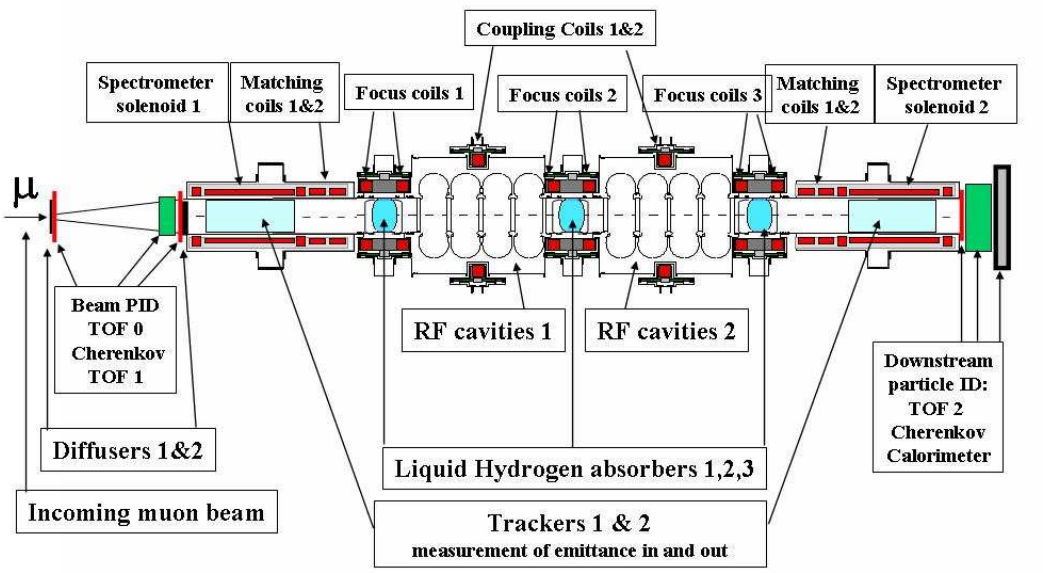

Figure 1: MICE Schematic.

A schematic overview of MICE is shown in Fig. 1. The MICE experiment consists of two trackers, which in itself consist of five superconducting solenoids each, two coupling coil modules and three absorber focusing coil modules. The superconducting magnets are required to steer the particles through the MICE channel onto liquid hydrogen absorbers. In the absorbers the muons collide with the hydrogen atoms, thus reducing their random particle motion (emittance reduction). The longitudinal momentum is restored in RF-cavities.

MICE will be assembled in several steps. At the time of writing it is aimed to finish construction of Step IV by summer/autumn 2014. MICE Step IV consists of two trackers and one AFC module. The various steps of MICE are shown schematically in Fig. 2. The coil geometries and current densities are described in the tables in appendix A.

The MICE solenoids produce a substantial amount of stray field, which is a concern as some of the technical equipment in the MICE hall may not work. Examples for this are cryo-cooler pumps, vacuum pumps or the tracker readout of the MICE experiment. An additional concern is the nearby ISIS control room, where the magnetic field has to be lower

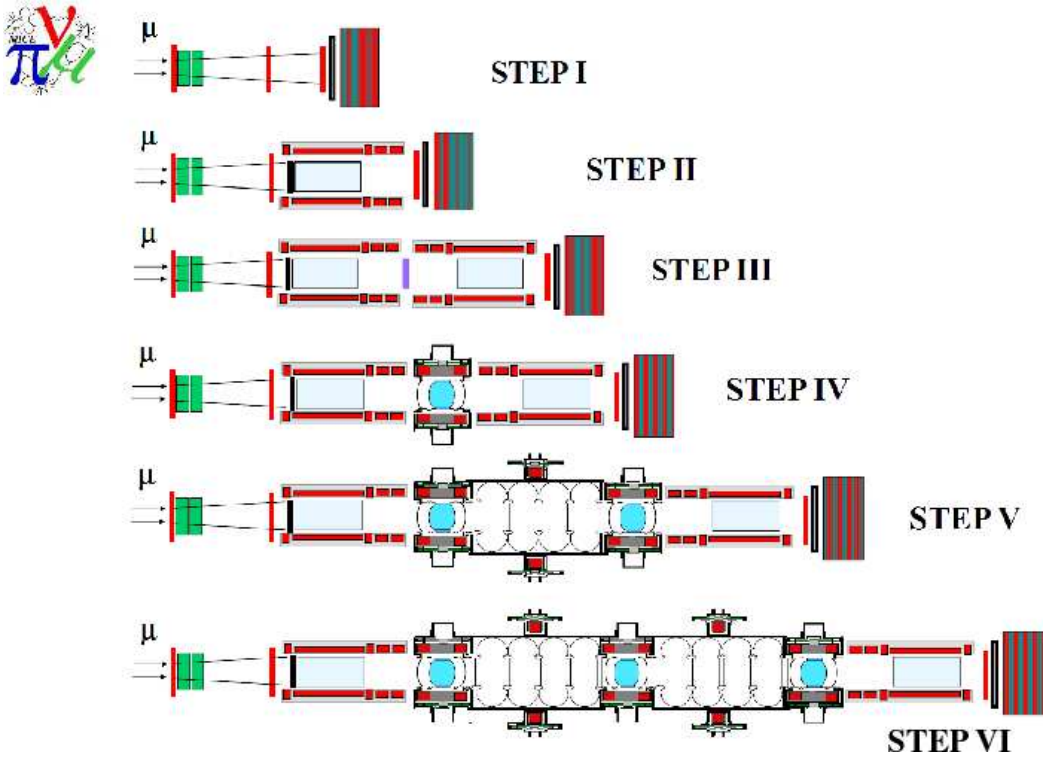

Figure 2: MICE Steps.

than 5 Gauss because of health and safety regulations. ISIS is UK's neutron spallation source.

In July a return yoke was presented to the MICE community, which partially encloses MICE. The partial enclosure is sufficient to reduce the stray fields to acceptable levels. This report describes the shielding concept, general engineering considerations and the expected performance.

2. Methodology - Computer Simulations

For the analysis of the problem and performance estimate two commercial finite element packages are employed: COMSOL Multiphysics[1] and Opera 3D from Cobham/Vectorfields[2]. In the simulations it is assumed that the yoke is made of AISI 1010 steel; the BH-data is taken from Opera, which is shown graphically in Fig. 3.

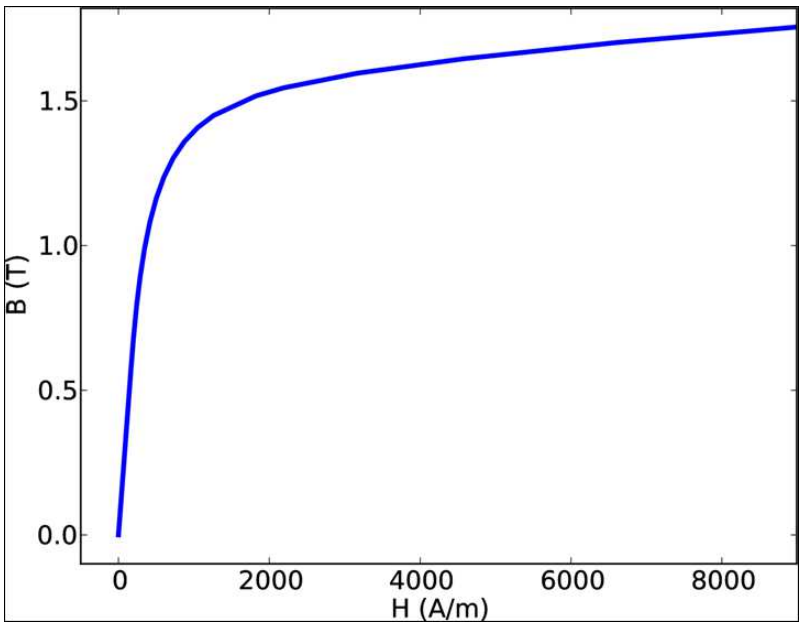

Figure 3: Magnetization curve of AISI 1010 steel.

The two software packages use different physics implementations, which allows to verify the obtained results. COMSOL solves for the magnetic vector potential:

$$\nabla \times \left(\mu^{-1} \nabla \times A\right) = J \ . \tag{1}$$

In this equation μ is the magnetic permeability, A the magnetic vector potential and J a current density. In contrast to this Opera 3D solves for the magnetic scalar potential ϕ:

$$\nabla \mu \nabla \phi - \nabla \mu \left(\int_{\Omega_J} \frac{J \times R}{|R^3|} \mathrm{d}\Omega_J \right) = 0 \ . \tag{2}$$

Contributions to the magnetic field from current carrying structures at a distance R are usually evaluated using Biot-Savart law and integrated over the domain Ω.

The advantage of the scalar potential implementation of Opera is that it is much more memory efficient: the number of degrees of freedom is smaller (scalar field versus vector

[1]COMSOL AB, Tegnergatan 23, SE-111 40 Stockholm, Sweden
[2]Cobham CTS Limited trading, 24 Bankside, Kidlington, Oxfordshire, OX5 1JE, UK

field for each point in 3D). The disadvantage is that problems are somehwat more difficult to setup, as different potentials need to be defined (reduced potential vs. total potential).

A special feature of COMSOL is the thin permeability boundary condition, which allows to model thin air gaps in geometries without compromising the mesh quality. This feature was benchmarked in a simulation with a real gap and no significant difference in the results was found. The thin permeability boundary condition can be described by the following equation:

$$n \times (H_1 - H_2) = \nabla_t \times \frac{d}{\mu_0 \mu_r} \nabla_t \times A \ . \tag{3}$$

In this equation H denotes the magnetic field strength and n a vector normal to the boundary.

In both software packages linear and quadratic elements were used, without observing a significant difference in the results. The final verification was usually carried out using quadratic elements, which results in a slightly better spatial resolution. In Opera the coil fields were evaluated by integration and the contributions from iron domains by nodal interpolation. This is the preferred evaluation mode according to the manufacturer (Cobham). The mesh size was chosen sufficiently small enough for the areas of interest, which was verified by mesh refinements and choosing higher order elements. For both simulation packages non-linear solvers were employed. Key proof-of-principle simulations were performed in both codes with for this application negligible differences in the results.

3. Concept

All MICE magnets are large diameter solenoids, which are relatively thin and short. From a shielding point of view an ideal solution is to encase the MICE magnets in a soft-iron cylinder. This is of course not practical; however, it is possible to achieve good shielding by only encasing MICE partially in this way. Fig. 4 shows the concept.

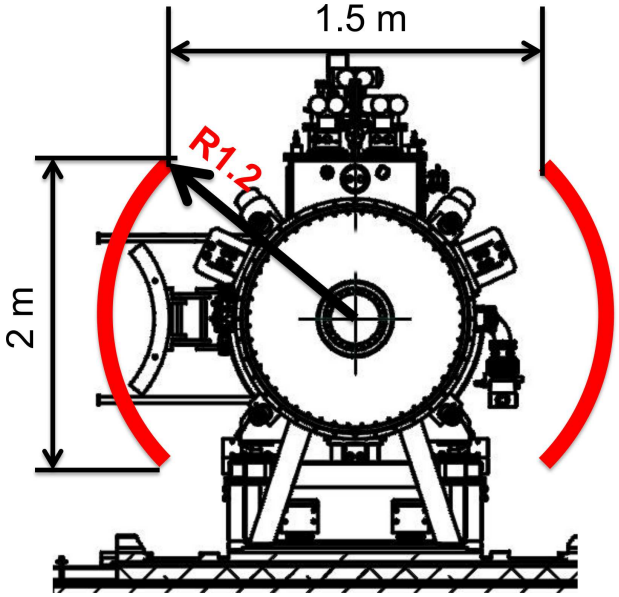

Figure 4: General Concept. The partial return yoke is shown in red.

As shown in the figure, the initial concept assumed soft-iron which is located on a circle with a radius of 1.2 m covering azimuthally $\pm 50°$. Initial studies showed that for Step IV a thickness of about 10 cm is required for good shielding. The weight of such a shield (which is about 8 m long) would be 30 tons (metric). The performance is shown in Fig. 5, which shows the modulus of the stray field on a surface with a radius of 1.5 m. The figure shows that the stray field is reduced to < 1.5 mT in the magnetic 'wind shadow' of the shield (without shield: more than 30 mT).

During the course of this project the shield has evolved; these changes either improved the performance of the shield or, at a later stage, were driven by engineering considerations. Figure 6 shows an overview of the development history.

The vertical extensions shown in the more recent design were added to provide a better suppression of the remaining stray field behind the shield, which originates in the uncovered parts of MICE. This is illustrated in Fig. 7, which shows flux tubes of the magnetic field. As shown, the flux tubes primarily stem from the top and the bottom openings in the shield. Adding these vertical extensions significantly improves the performance, which is shown in Fig. 8. The figure shows a side-by-side comparison: using vertical extensions the magnetic field can be reduced to less than 1 mT. At the same time the good field region

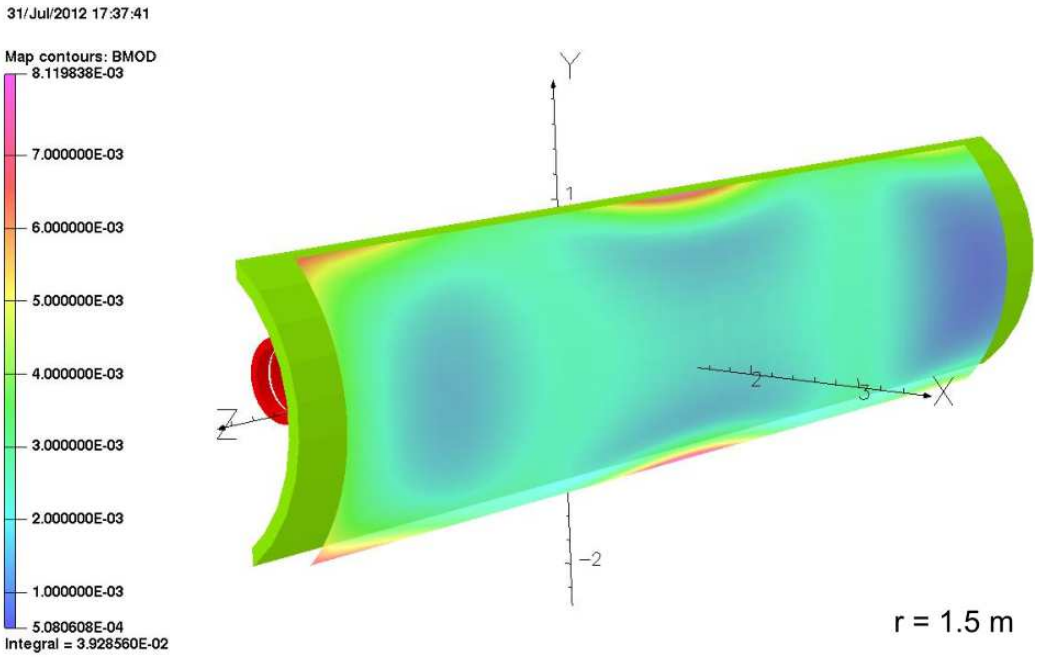

Figure 5: General Concept - Performance.

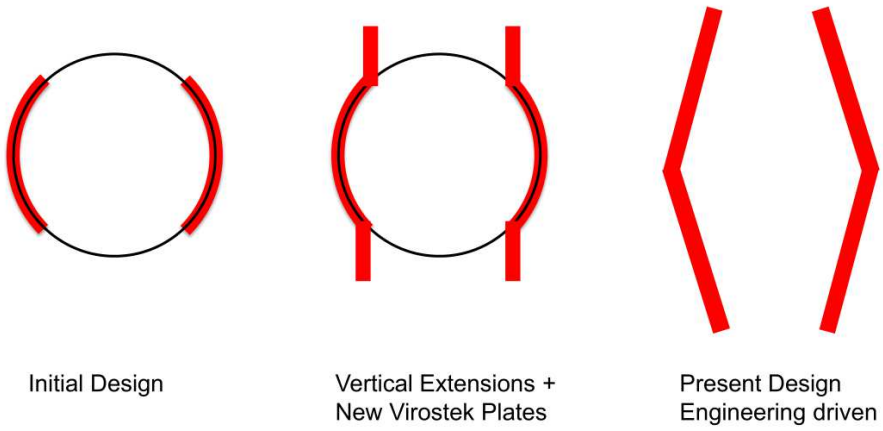

Figure 6: Development History

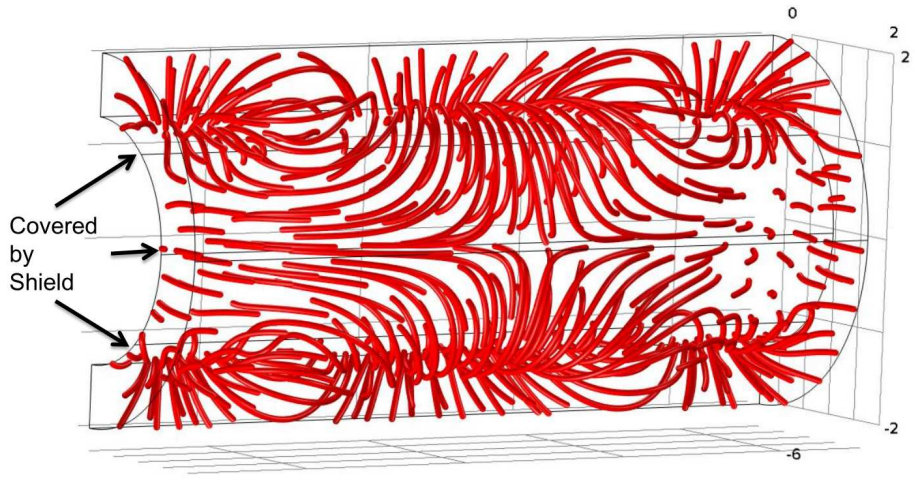

Figure 7: Source of Stray Field.

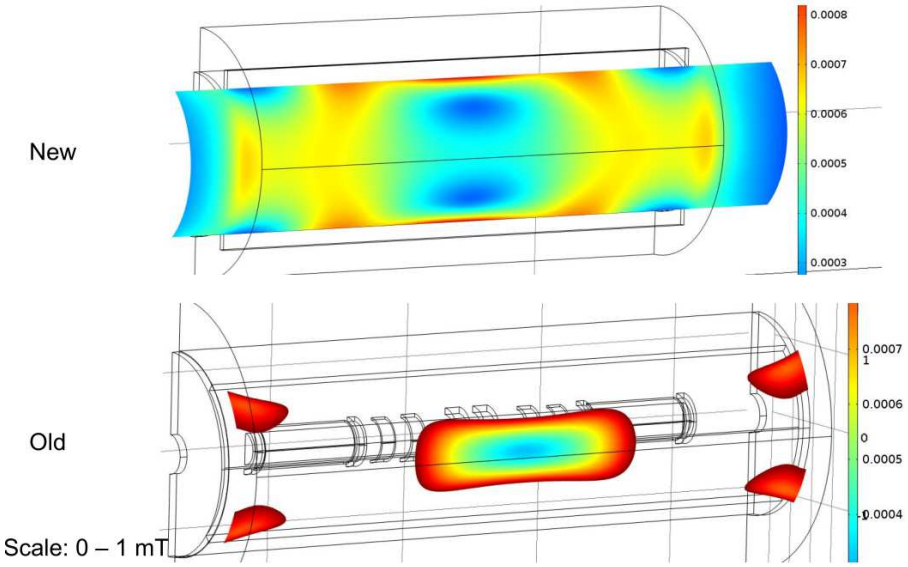

Figure 8: Comparison Vertical Extension. Both pictures use the same scale for the magnetic flux density.

is increased.

This report will primarily discuss the latest version, which is shown in Figure 6 on the right. While showing a good performance, the early shapes of the shield were too costly and time consuming to manufacture. The shield was therefore modified to employ straight panels.

4. Engineering

The engineering design of the magnetic shield was carried out by the Mechanical Engineering group of the Magnet Division at BNL. In this report we summarize the efforts of the initial design phase, which includes the general engineering concept, the support structure, forces on shield and connection issues.

4.1. Engineering Concept

Figures 9 and 10 show the general engineering concept. Early on it was established that the arc shaped shield design is expensive to manufacture and was therefore modified to be compatible with sheet material. The emerged design has a very similar if not better shielding characteristic in comparison to the initial suggestion with vertical extensions. In total 8 panels of AISI 1010 are required, each about 4 m long and 1.5 m in width. The thickness of each panel is 10 or 12 cm, depending on the desired shielding performance (see performance section). The weight of each panel is approximately 4.5 t (metric) and can therefore be lifted and transported in the MICE hall (the cranes in the MICE hall have a weight limit of 8 tons). Each panel is tilted by 11.5° to interfere less with components in the hall and to improve the shielding performance.

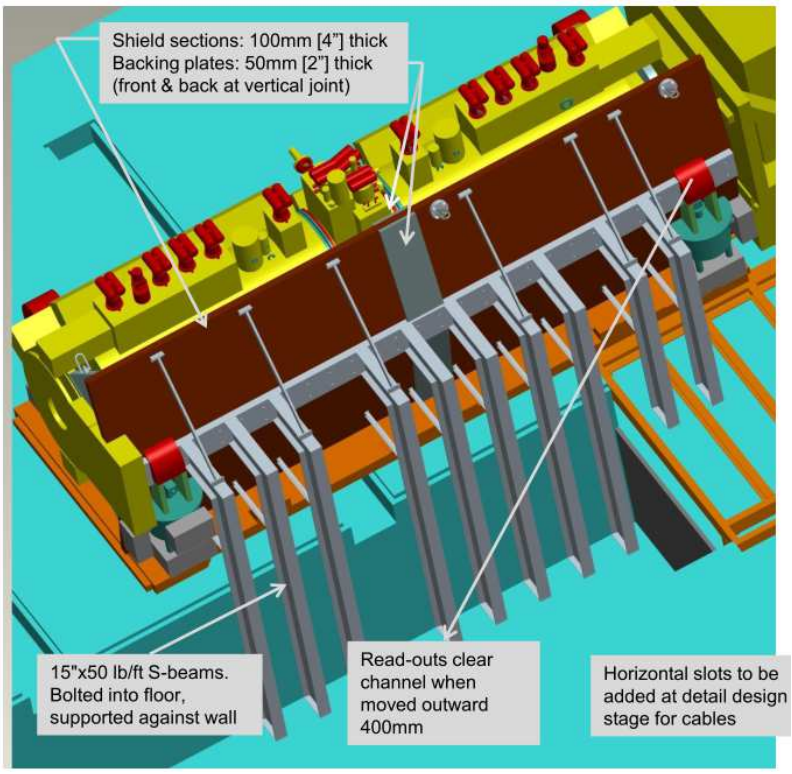

Figure 9: Overview of the engineering design.

Fig. 10 shows the shield and support structure, which consists of several S-beams. The support structure is designed to take the force acting on the shield to the floor. The number of support legs has been adjusted to comply with maximum permissible floor loadings in the MICE hall in this area.

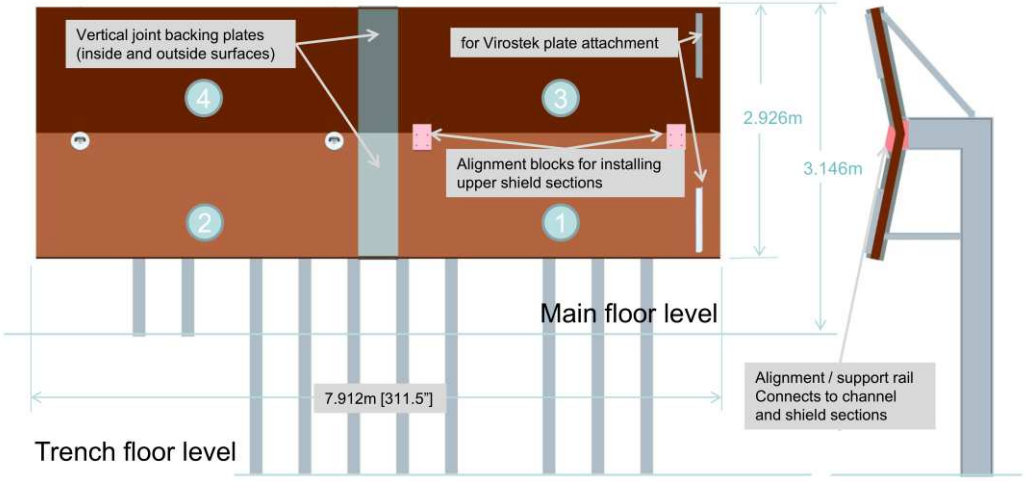

Figure 10: The MICE Partial Return Yoke.

An additional iron structure is envisaged to cover the open space between the Virostek plate and the shield, which further improves the shielding performance by preventing flux leakage.

4.2. Forces on the Shield

The forces on the shield were evaluated for all cases of Step IV. The study was carried out using COMSOL, which allows to evaluate the force using the Maxwell stress tensor. The force is evaluated for each panel separately (for the panel numbering see Fig. 11).

Table 1 shows the results of the analysis. It is worth nothing that there is no net longitudinal or vertical force on the shield due to symmetry reasons. The largest force is in horizontal direction; the direction is such that it acts to collapse the shield onto the MICE channel.

The forces were used to evaluate the stresses and deflection of the shield. The forces were applied as a bulk force in an ANSYS FEA simulation. The results of this simulation are shown in Fig. 12. The maximum deflection is 5 mm, which occurs at the top of the shield. This can be reduced significantly by either doubling up the S-beams (reduction of factor two) or by introducing crossbars (to less than 0.011" or 0.28 mm). Crossbars were adopted for the following engineering design.

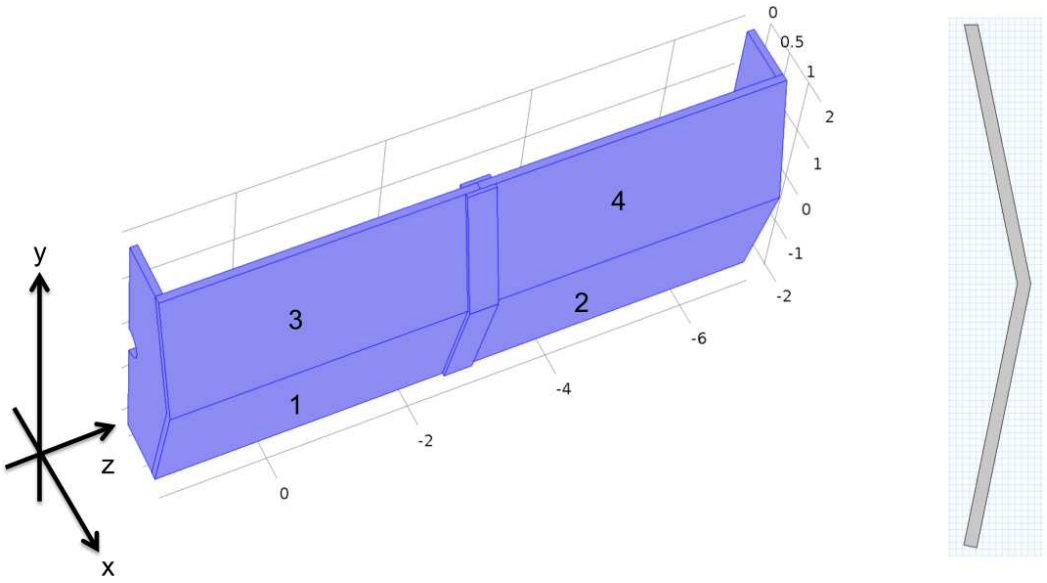

Figure 11: Geometry used to evaluate the forces on the shield.

Table 1: Forces on the shield in Newton.

	200 MeV Flip	240 MeV Flip	200 MeV Solenoid	240 MeV Solenoid	Case 5 Solenoid
Section 1 F_x	-7376.33	-8460.42	-2344.79	-2258.92	-3077.52
Section 1 F_y	1432.616	1645.391	436.8723	416.7314	575.7667
Section 1 F_z	-0.47088	0.249875	436.8723	-3.05458	-7.45149
Section 2 F_x	-7414.04	-8498.62	-2382.47	-2297.38	-3115.83
Section 2 F_y	1439.288	1651.915	444.0151	423.9587	582.4661
Section 2 F_z	2.222123	2.005446	444.0151	3.3193	7.713439
Section 3 F_x	-7375	-8458.57	-2344.89	-2258.96	-3077.52
Section 3 F_y	-1432.93	-1645.79	-436.749	-416.659	-575.815
Section 3 F_z	-1.48953	-0.75518	-436.749	-3.73833	-7.96631
Section 4 F_x	-7415.2	-8500.02	-2382.9	-2297.8	-3116.01
Section 4 F_y	-1441.16	-1654.05	-444.725	-424.701	-583.916
Section 4 F_z	1.914087	1.318587	-444.725	3.487784	7.683155

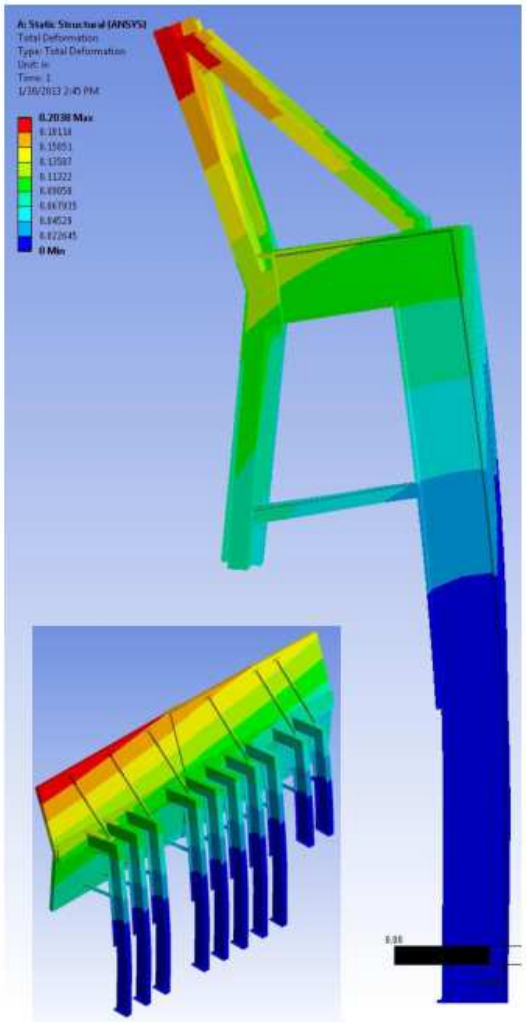

Figure 12: Result of the ANSYS simulation.

4.3. Vertical Gaps in the Shield

Vertical gaps in the shield occur between two adjacent shielding panels. Initial investigations showed that vertical gaps in the shield are detrimental for the shielding performance. Fig. 13 shows the position of a vertical gap in the shield near the tracker region. The simulation result of the stray magnetic flux behind the shield at a radius of 1.5 m (beam height) is shown in Fig. 14. The figure shows that depending on the width of the gap the stray field behind the shield increases substantially.

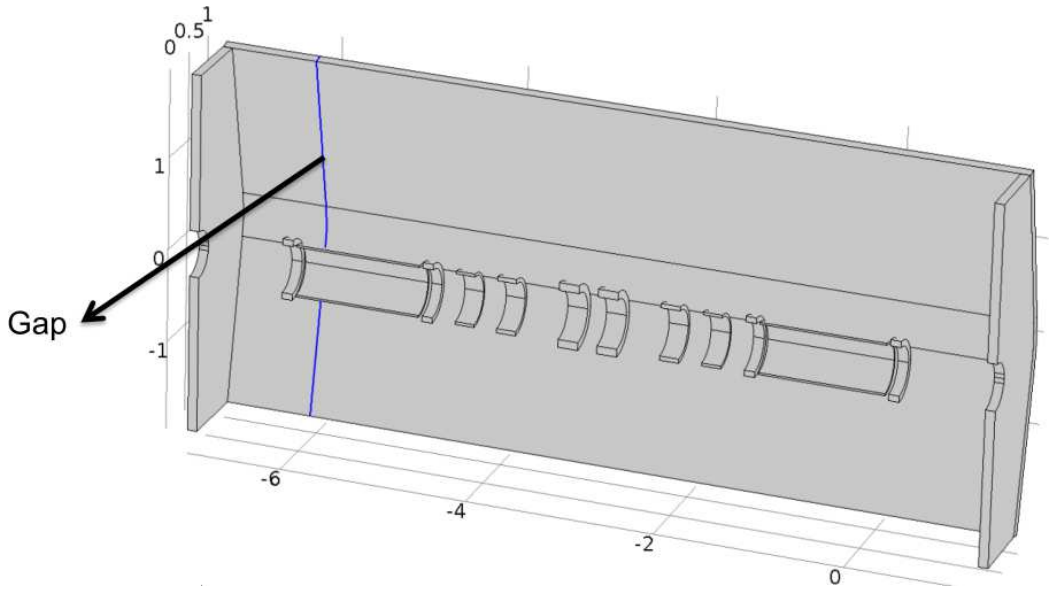

Figure 13: Geometry: Vertical gap in shield.

To avoid performance impacts several potential solutions were studied. An adequate and easy to implement strategy is to double-up the shield at the position of a vertical gap; Fig. 15 illustrates the concept. Each of the two backing plates is required to be half the thickness of the shield. The width of each connection piece is 0.4 m. The backing plates work by forming a low magnetic reluctance joint between neighboring shield sections; at the joint the magnetic flux is redirected into the backing plates, thus avoiding the vertical gap. The performance of this concept was evaluated using FEA; in the simulation it was assumed that the air gap between backing plates and shielding panel is 0.5 mm. As shown in Fig. 16, the impact on the shielding performance can be expected to be minimal.

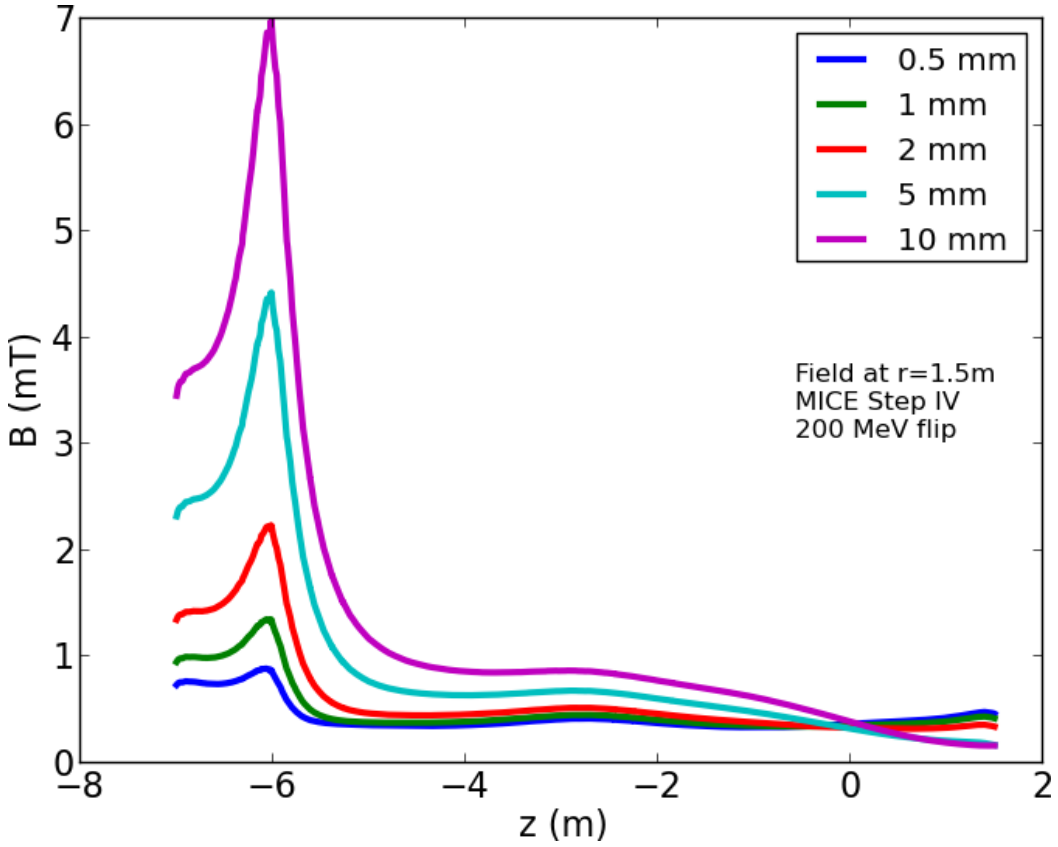

Figure 14: Modulus of the magnetic flux density at a radius of 1.5 m for 200 MeV flip mode assuming a vertical gap at $z = -6$ m.

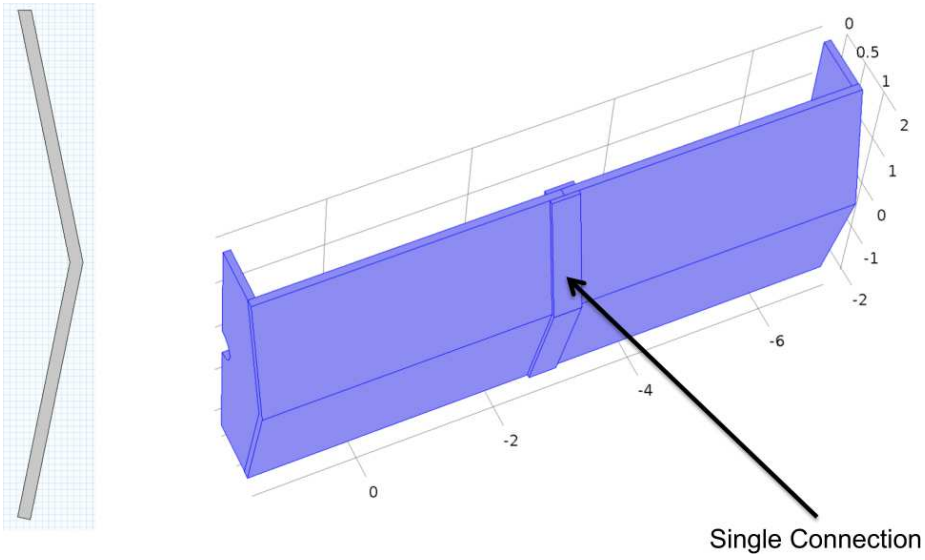

Figure 15: Concept of doubling up a vertical gap.

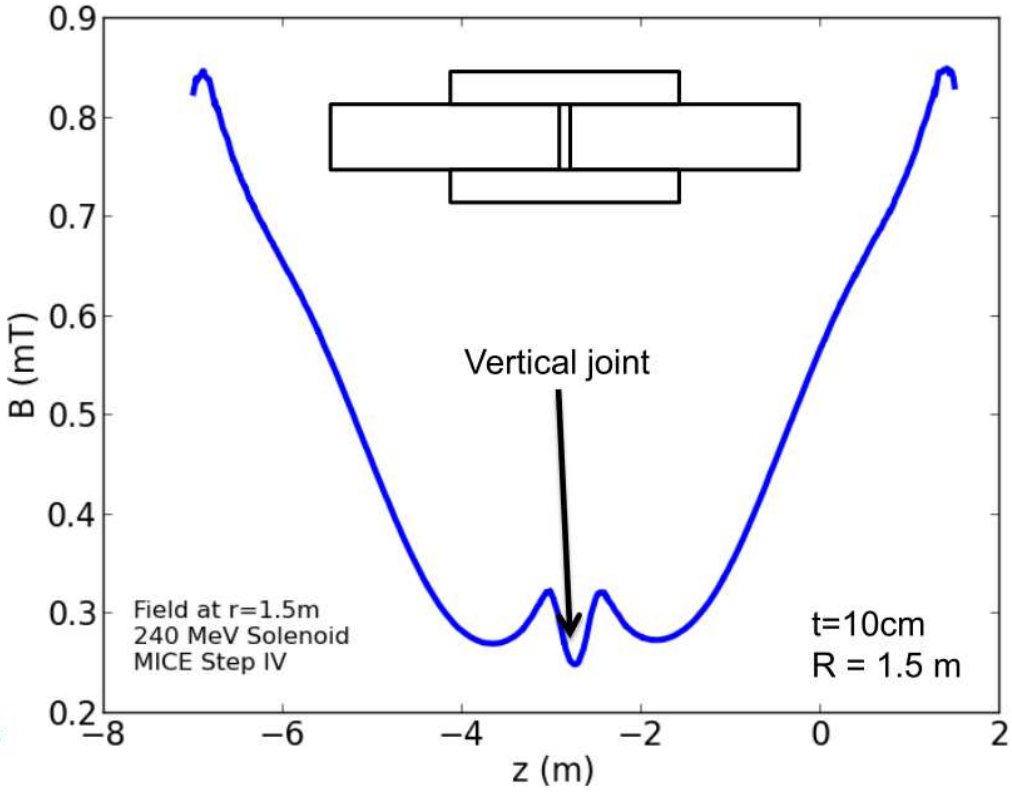

Figure 16: Modulus of the residual stray field at a radius of 1.5 m (beam height) for 200 MeV flip mode. The vertical gap is doubled up using to backing plates, each 40 cm long.

4.4. Horizontal Gaps in the Shield

Horizontal gaps as shown in Fig. 17 in the shield were studied as well. Fig. 18 and Fig. 19 show simulation results for 200 MeV flip mode. The figures show that the stray field behind the shield by comparison is far less sensitive to horizontal gaps. Even gaps of 20 cm width produce only an increase in stray field of about 1 mT. Horizontal slots in the shield as shown in Fig. 20 can therefore be used for feedthroughs.

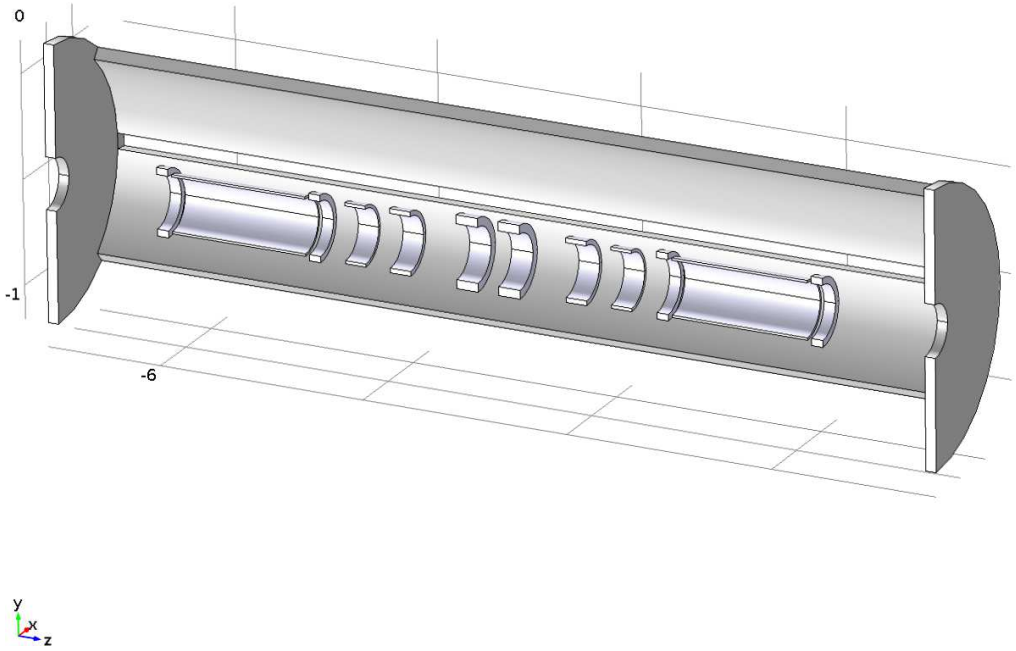

Figure 17: Horizontal gap in shield: Geometry Overview.

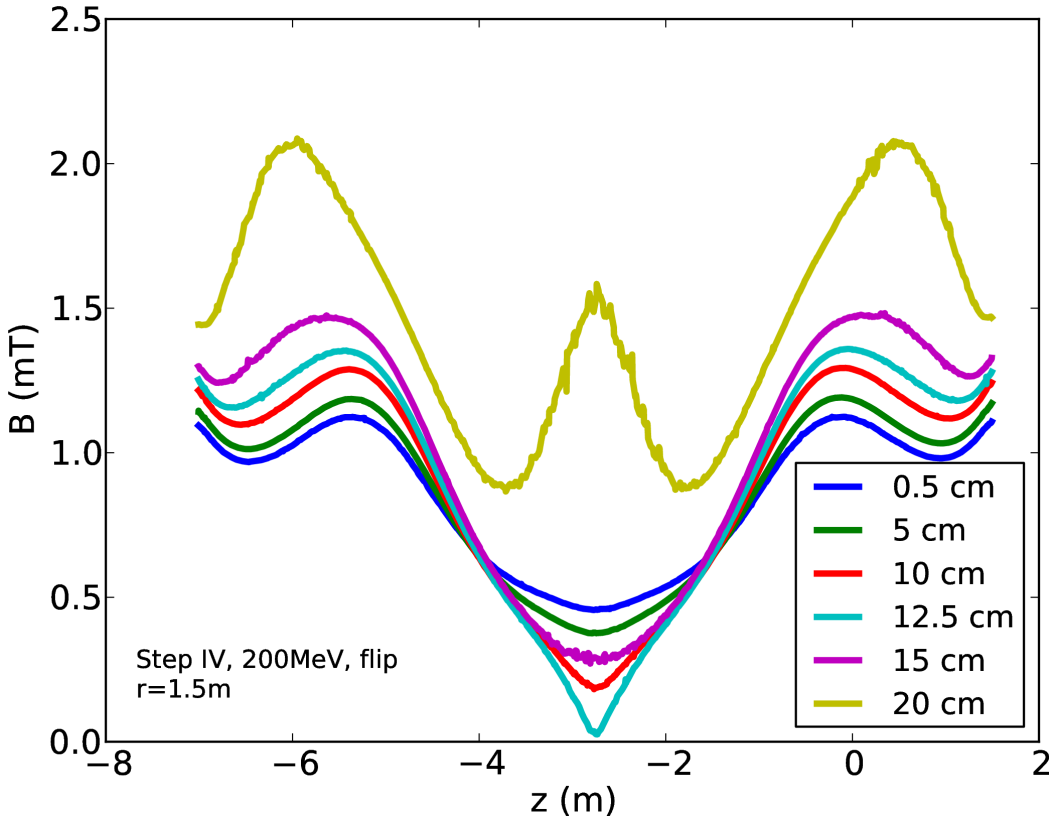

Figure 18: Modulus of the residual magnetic field at a radius of 1.5 m. The simulation assumes a horizontal gap in the shield at beam height.

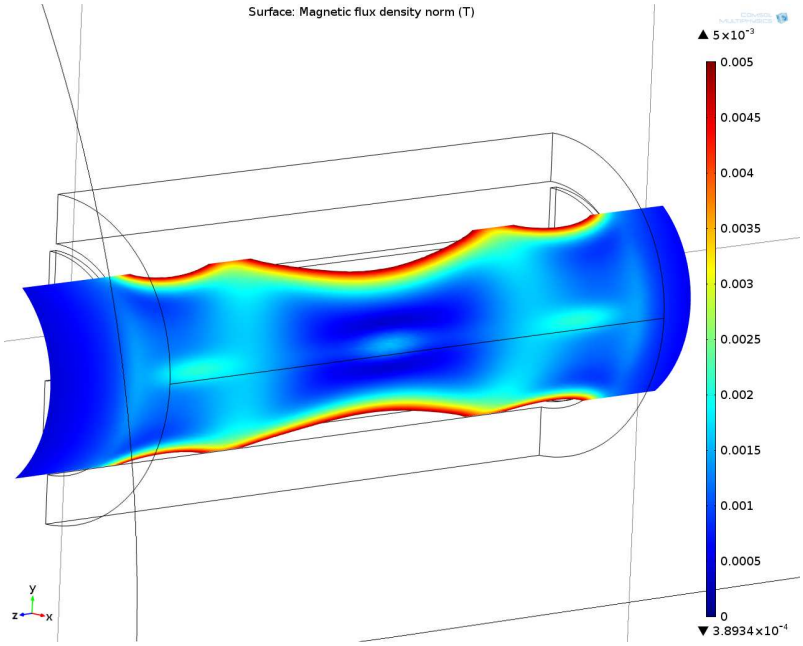

Figure 19: Field at a radius of 1.5 m behind the shield. This simulation assumes a horizontal gap of 200 mm width over the entire length of the shield (see Fig. 17).

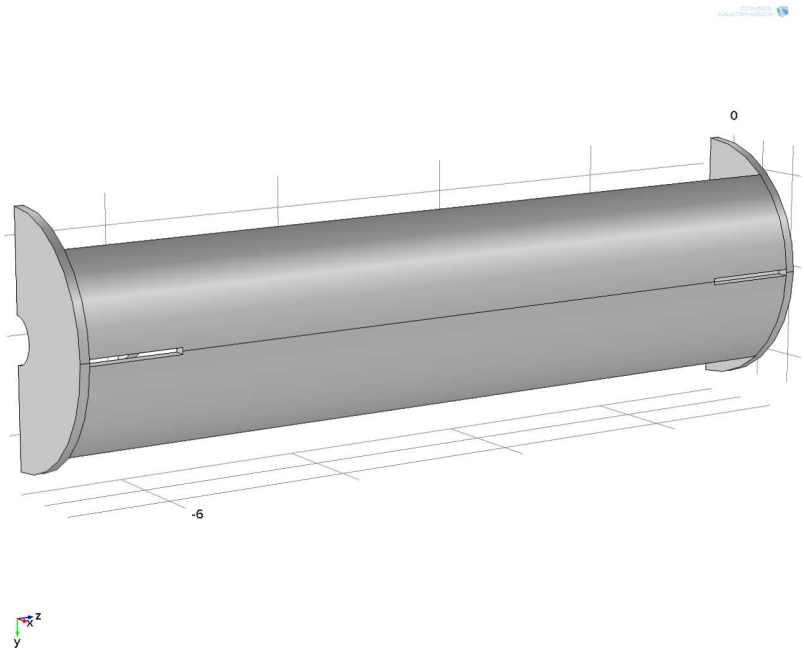

Figure 20: The figure shows a shielding concept with a 1 m long slot near the tracker region, which can be occupied by the tracker waveguides to connect tracker and tracker cryostat. The slots are 10 cm wide, which is sufficient for the tracker wave guide connectors.

4.5. Nested Shields – An Additional Approach

An alternative approach was initially considered, which is that of nested shields at different radii. The approach is shown schematically in Fig. 21. The radial gap between the two shields can be used for feedthroughs; initial performance studies showed a negligible effect on the shielding performance. Given that the slot approach discussed earlier is more practical and almost certainly cheaper to realize, this approach was not considered further.

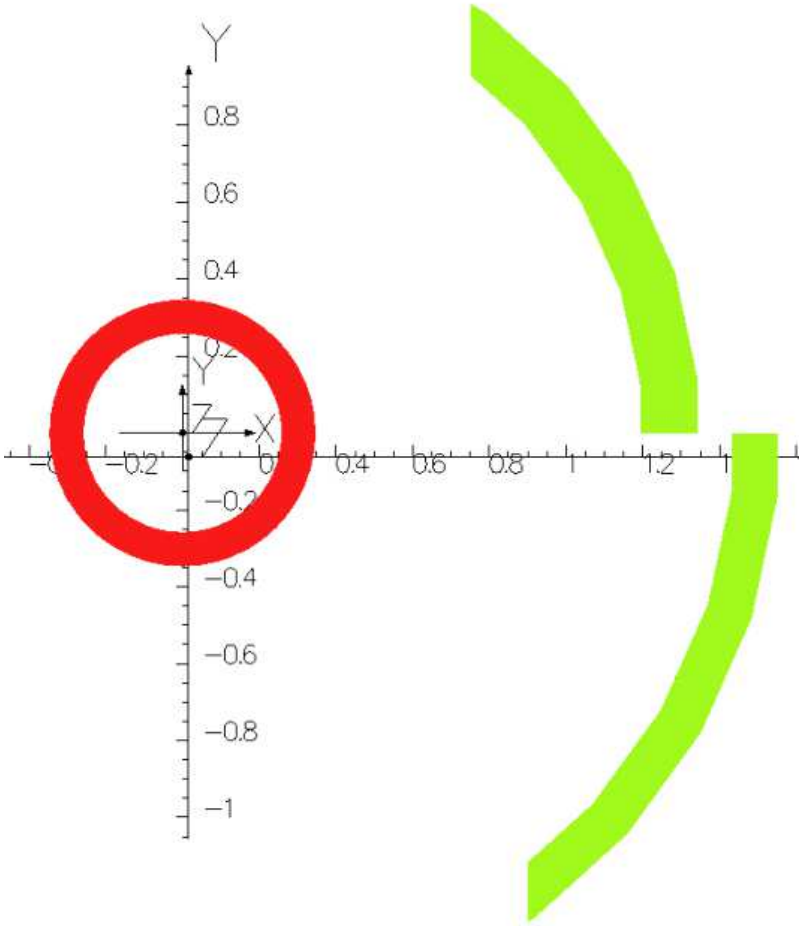

Figure 21: Concept for feedthrough of connectors.

5. Expected Performance

For the design care was taken to keep the magnetization in the partial return yoke around 1.25 T, which is the level where μ_r starts to decrease. Fig.22 shows the typical magnetization in the shield for the 200 MeV flip mode.

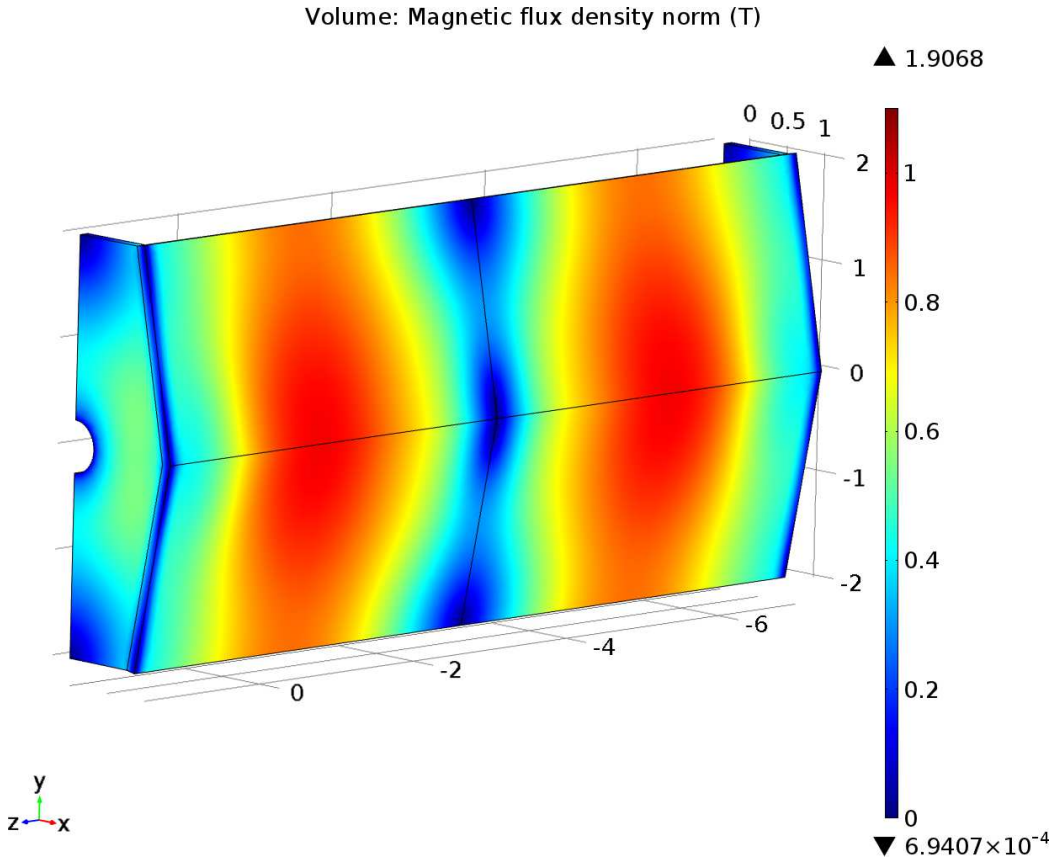

Figure 22: Magnetic field equivalent to the magnetization of the shield for 200 MeV in flip configuration.

The aim of the shield is to screen large parts of the MICE hall from stray fields higher than about 5 Gauss. This level is sufficient for the operation of magnetically sensitive equipment such as cryopumps, power supplies and vacuum gauges located in the tracker cryostat. Fig. 23 show the magnitude of the magnetic field at a radius of 1.5 m (just behind the shield) at beam height. The figure shows the magnetic field without shield for flip and solenoid mode (both 240 MeV). The expected stray field with shield is shown for two shield ticknesses, which are 10 and 12 cm. For the shielded case the 240 MeV solenoid mode is chosen, which can be considered a worst case. The figures show that the stray field is reduced from 30-60 mT to about 1 mT in case of the 10 cm shield and less than 0.6 mT for the 12 cm shield; this is a reduction of factor 30–100, depending on the position and

chosen shield thickness. This means that an increase of the shielding iron by 20% leads to about twice the performance.

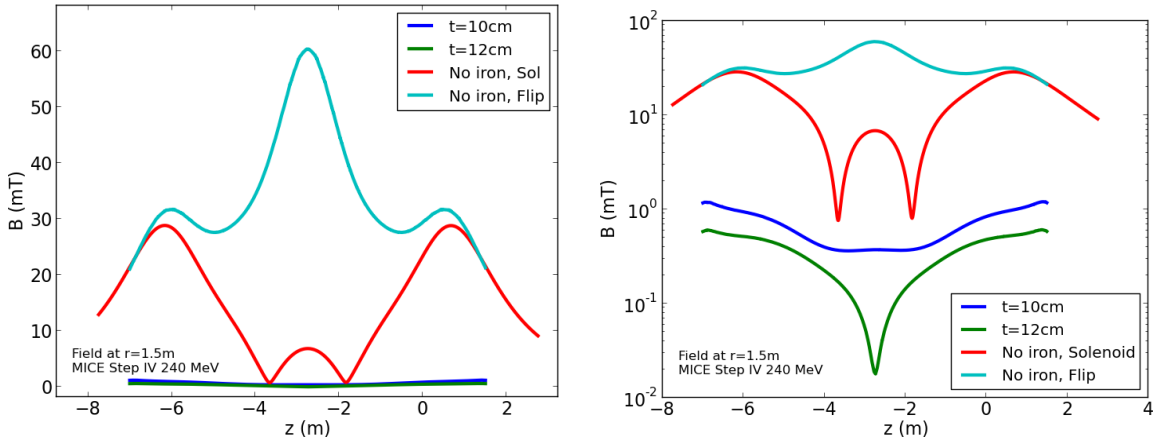

Figure 23: Modulus of the magnetic fringe field at a radius of 1.5 m at beam height. Both figure show the same data; the figure of the right hand side uses a logarithmic scale.

Fig. 24 and 25 show the extent of the fringe field for the 200 MeV flip mode. The pictures show 3D iso-surface plots; the green surface represents a field of 5 Gauss. Both figures show a comparison of the unshielded situation versus the stray field extent with partial return yoke. The unshielded scenario assumes no iron in the MICE hall (such as walls or the floor). The figures emphasize that the stray field extent is drastically reduced with the magnetic shield: in longitudinal direction the stray field is reduced from about ± 7.5 m to about half of that. Even in vertical direction, which is not covered by the shield, the stray field extent is reduced significantly from 9 m to about 4.5 m. In horizontal direction the 5 Gauss line (assuming a 12 cm thick shield) is located right behind the shield, which means in the MICE hall the field is lower than this.

Particular emphasis during the development process was on a solution which would ensure that equipment vital to the operation of MICE was shielded. In particular, the electronics within the tracker cryostats are known to be very sensitive to magnetic field. The tracker cryostats are located adjacent to the two tracker magnets. Without shield the stray field is around 36 mT as shown in Fig.26. Using the shield this is reduced to 0.6 mT or 6 Gauss at the position closest to the tracker. The stray field within the tracker cryostat drops quickly with distance, so on the opposite side of the cryostat the field is predicted to be less than half of this (< 3 Gauss).

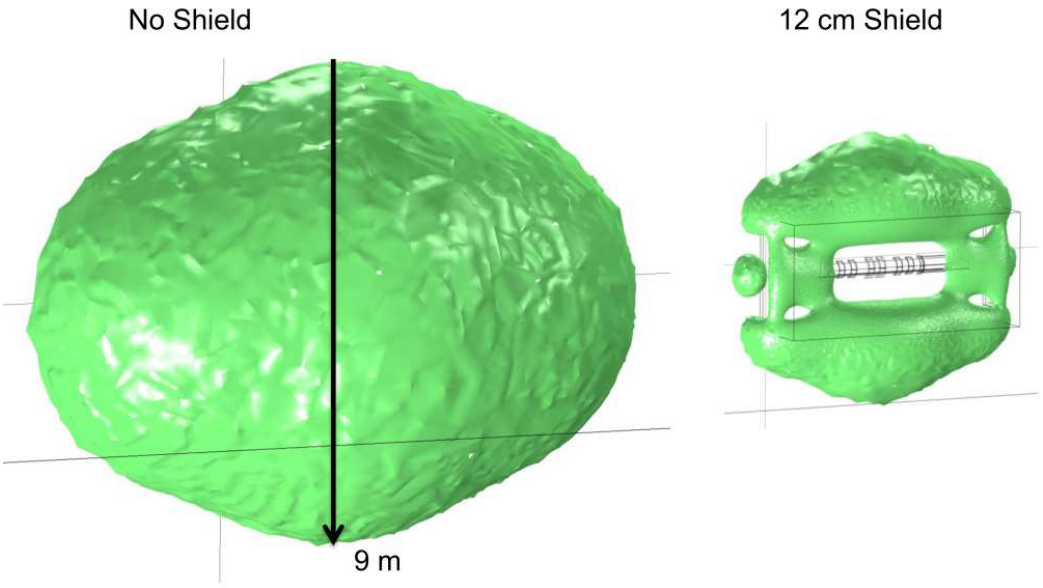

Figure 24: 5 Gauss iso-surface plot of MICE for the 200 MeV flip mode. The left figure shows the 5 Gauss surface for an unshielded scenario (no iron present) versus the case where the shield is adopted.

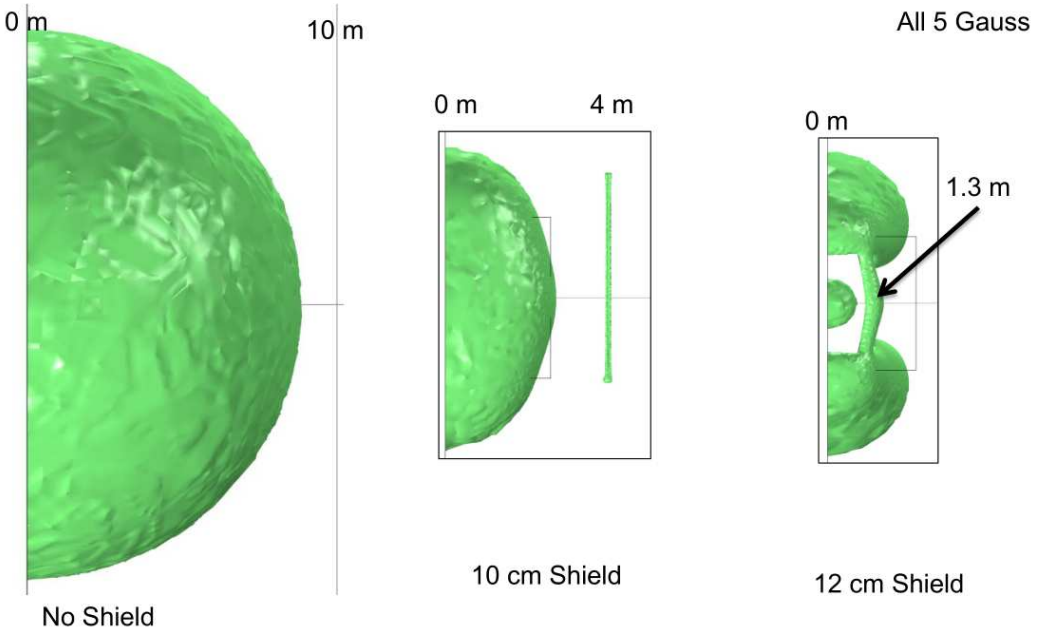

Figure 25: 5 Gauss iso-surface plot of MICE for the 200 MeV flip mode, shielded and unshielded, in frontal view.

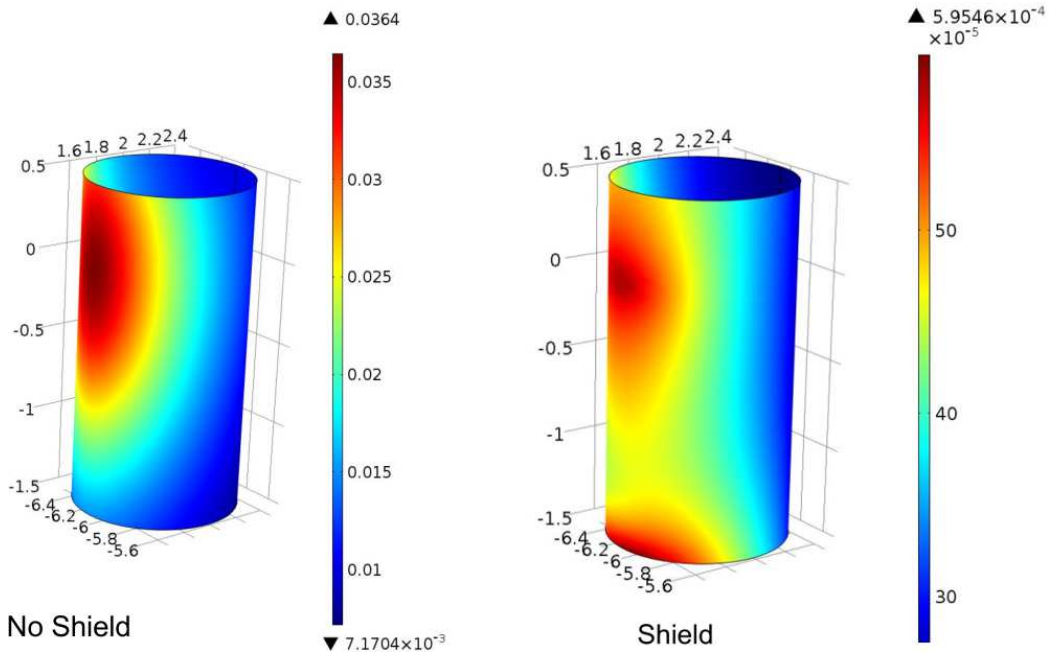

Figure 26: Modulus of the magnetic field at the position of the tracker cryostat. The left figure shows the field assuming an unshielded situation and the right one with a 12 cm thick shield.

6. Effect On the Beam

The effect of the MICE shield on the beam dynamics of MICE was studied separately using tracking studies in MAUS. The findings are discussed in more detail in [2]; in short the study concluded that the partial return yoke has a barely measurable effect on the beam travelling through MICE. The main effect is to introduce a slight misfocus to the beam, introducing a slight change in the cooling power of the channel. In summary, there is no reason, from a beam dynamics perspective, not to implement the partial return yoke.

7. Extension to Step VI

The main focus of the development process is on Step IV. However, an important side aspect of the development was the possibility to upgrade the design to Step VI. Step VI is presently expected to commence in 2018[1]. Step VI is more challenging to shield than Step IV due to the presence of the large coupling coils. It is generally accepted that local shielding, that is shielding of individual components, will not work in all likelihood. A limited effort was therefore made to show that the partial return yoke can also be implemented for Step VI. A potential geometry of the partial return yoke is shown in Fig. 27. The residual stray field at a radius of 1.8 m, which is just behind the shield, is shown in Fig. 28. The figure illustrates that a similar shielding efficiency can be obtained for Step VI as well.

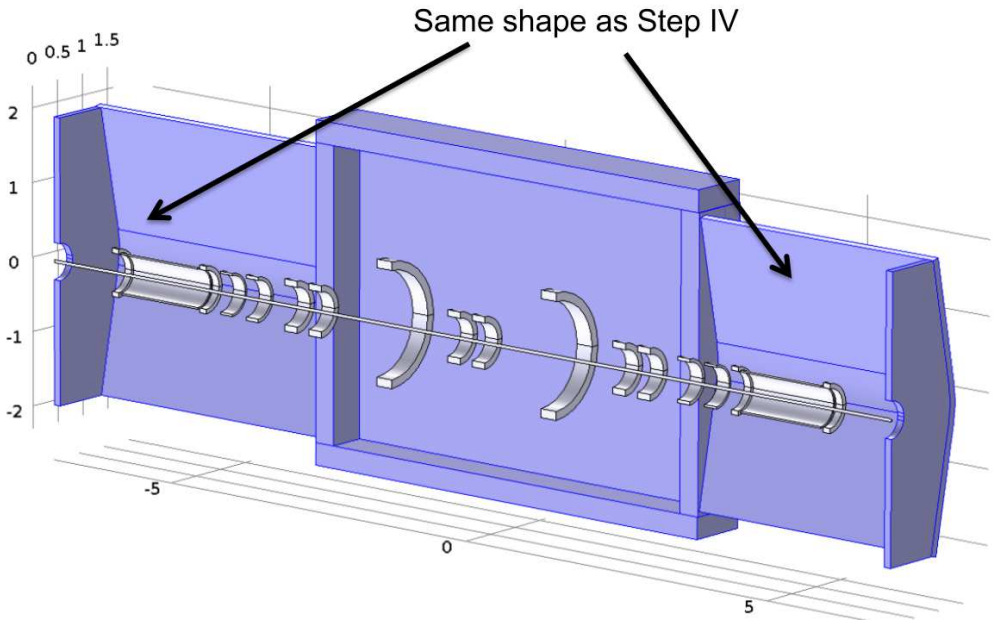

Figure 27: Suggested shield geometry for Step VI.

In general it was tried to recycle as much as possible of Step IV; the region in Step VI which offers itself to this is the tracker region, where the iron panels of the Step IV shield can be used. Around the coupling coils new iron panels (not shaped) would need to be installed. Preliminary simulations showed that the iron near the coupling coils needs to be at least 30 cm thick for sufficient shielding. The increase in thickness is due to the larger amount of magnetic flux generated in this area. Fig. 29 and 30 show the extent of the 5 Gauss surface in 3D iso-surface plots.

The figures illustrate that the shield can reduce the stray field in the MICE hall effectively: longitudinally the 5 Gauss line shifts from ± 20 m to ± 7.5 m and finishes with the MICE experiment. In vertical direction the extent of the fringe field is reduced from 15 to

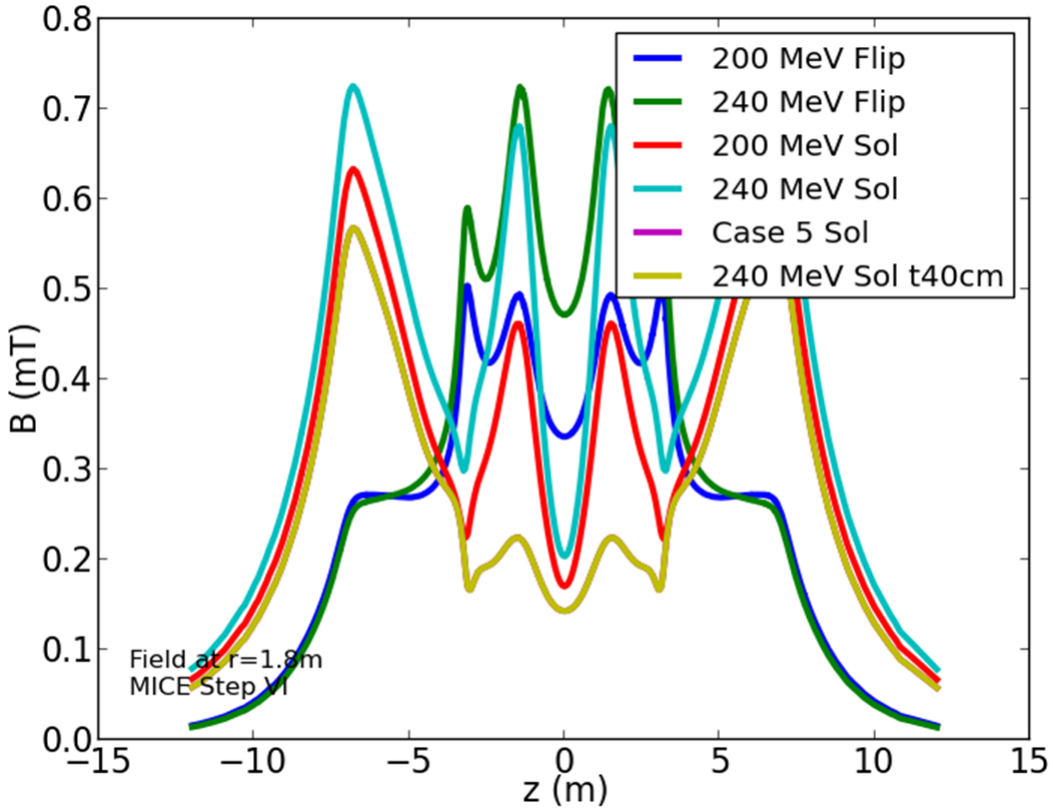

Figure 28: Residual stray field (modulus) at a radius of 1.8 m for the various cases of Step VI.

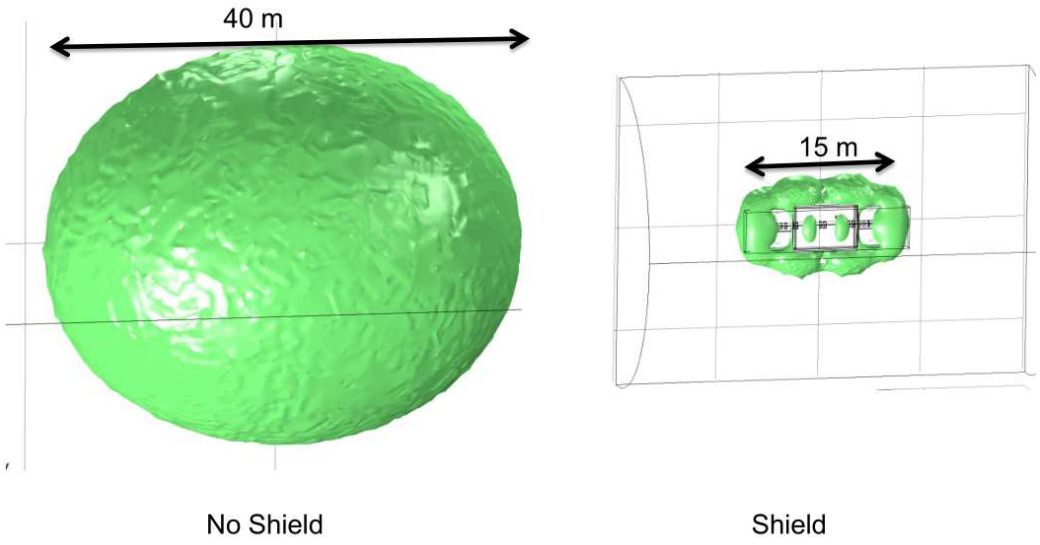

Figure 29: Step VI: iso-surface plot of the 5 Gauss line (with and without shield).

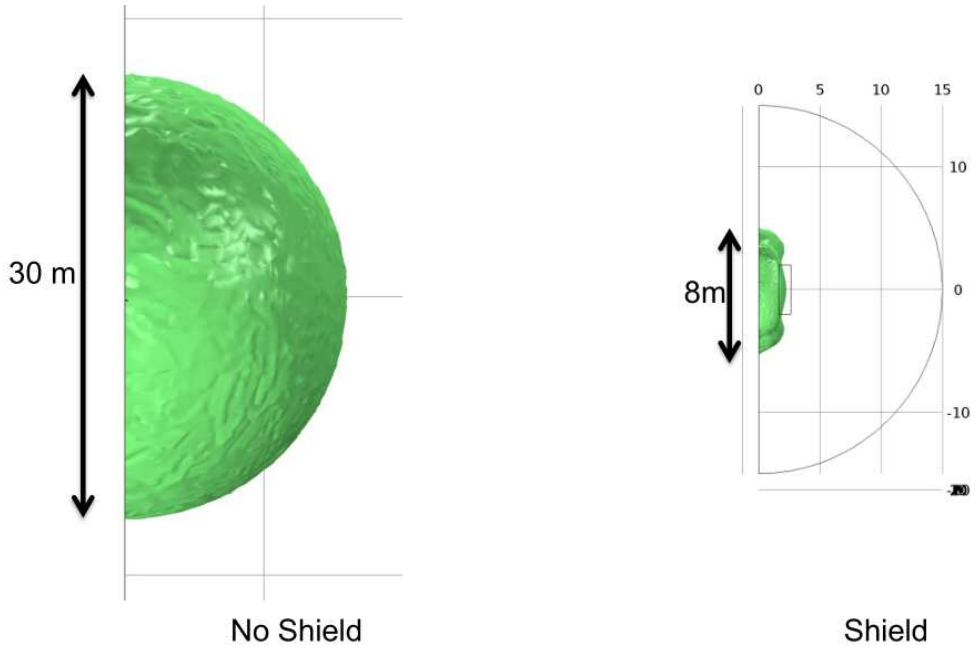

Figure 30: Step VI: iso-surface plot (frontal view) of the 5 Gauss line (with and without shield).

4 m. Horizontally the 5 Gauss surface moves effectively to the position of the shield, that is the fringe field in the hall is reduced to 5 Gauss or less.

8. Conclusion

This report summarizes activities of the initial design phase of a magnetic shield (partial return yoke) for the Muon Ionization Cooling Experiment (MICE) in the UK. Finite element simulations predict that this concept is capable of reducing the stray field level in the MICE hall to safe levels (6 Gauss or less, which is about 1% of the initial stray field). The remaining stray field should be safe for operation of electric and electronic equipment.

While most of the efforts concentrated on Step IV, it was also shown that in principle this shielding approach is compatible with Step VI. The shielding panels of the shield in Step IV can be recycled for protecting the trackers in Step VI. Near the coupling coils new panels are required. In this area due to the larger radius and hence increased magnetic flux significantly more iron is needed for adequate shielding.

A large emphasis during the initial design phase was on engineering; progress has been made on the general feasibility and structural analysis. This includes force, stress and displacement calculations. A support structure was designed which can deal with the forces. Further progress was made on critical engineering questions such as unavoidable gaps in the shield if made of several parts. Suggestions for mitigation were made as well. Furthermore, a cost estimate was obtained for the partial return yoke design, which also includes a time estimate for production and assembly.

At the time of writing the detailed design phase for the partial return yoke was launched and is expected to be finished by mid 2013.

References

[1] A. Blondel. Cm 34 wrap-up. Talk at MICE Collaboration Meeting 34, October 2012. http://tinyurl.com/cl9td6t.

[2] C. Rogers and H. Witte. Effect of iron partial return yoke on the mice beam. MICE Analaysis Meeting, January 2013. http://micewww.pp.rl.ac.uk/issues/1161.

[3] H. Witte. Software model verification. Talk at MICE Magnetic Shielding Meeting, November 2012. http://tinyurl.com/c7qzccx.

[4] H. Witte. Step iv & vi: Local flux return. Talk at MICE Collaboration Meeting 34, October 2012. http://tinyurl.com/boh322s.

[5] H. Witte. Update on shield. Talk at MICE Magnetic Shielding Meeting, November 2012. http://tinyurl.com/cv3d5da.

[6] H. Witte. Azimuthal gaps. Talk at MICE Magnetic Shielding Meeting, January 2013. http://tinyurl.com/cmpdoqt.

[7] H. Witte. Racks and compressors. Talk at MICE Magnetic Shielding Meeting, January 2013. http://tinyurl.com/d69ocsr.

A. Coil Configurations

A.1. Step IV

Table 2: Step IV, 200 MeV Flip Mode

	z1 [m]	z2-z1 [m]	r1 [m]	r2 [m]	J [A/mm^2]
1	-6.0063	0.1106	0.258	0.324	-135.18
2	-5.8582	1.3143	0.258	0.2793	-152.44
3	-4.5063	0.1106	0.258	0.3176	-127.37
4	-4.1508	0.1995	0.258	0.2878	-137.13
5	-3.7116	0.2012	0.258	0.3027	-118.56
6	-3.06	0.21	0.263	0.347	-113.95
7	-2.65	0.21	0.263	0.347	113.95
8	-1.99	0.2012	0.258	0.3027	118.56
9	-1.549	0.1995	0.258	0.2878	137.13
10	-1.1104	0.1106	0.258	0.3176	127.37
11	-0.956	1.3143	0.258	0.2793	152.44
12	0.3967	0.1106	0.258	0.324	135.18

Table 3: Step IV, 240 MeV Flip Mode

	z1 [m]	z2-z1 [m]	r1 [m]	r2 [m]	J [A/mm^2]
1	-6.0063	0.1106	0.258	0.324	-135.18
2	-5.8582	1.3143	0.258	0.2793	-152.44
3	-4.5063	0.1106	0.258	0.3176	-127.37
4	-4.1508	0.1995	0.258	0.2878	-151
5	-3.7116	0.2012	0.258	0.3027	-142
6	-3.06	0.21	0.263	0.347	-137
7	-2.65	0.21	0.263	0.347	137
8	-1.99	0.2012	0.258	0.3027	142
9	-1.549	0.1995	0.258	0.2878	151
10	-1.1104	0.1106	0.258	0.3176	127.37
11	-0.956	1.3143	0.258	0.2793	152.44
12	0.3967	0.1106	0.258	0.324	135.18

Table 4: Step IV, 200 MeV Solenoid Mode

	z1 [m]	z2-z1 [m]	r1 [m]	r2 [m]	J [A/mm^2]
1	-6.0063	0.1106	0.258	0.324	135.18
2	-5.8582	1.3143	0.258	0.2793	152.44
3	-4.5063	0.1106	0.258	0.3176	127.37
4	-4.1508	0.1995	0.258	0.2878	55
5	-3.7116	0.2012	0.258	0.3027	62
6	-3.06	0.21	0.263	0.347	60
7	-2.65	0.21	0.263	0.347	60
8	-1.99	0.2012	0.258	0.3027	62
9	-1.549	0.1995	0.258	0.2878	55
10	-1.1104	0.1106	0.258	0.3176	127.37
11	-0.956	1.3143	0.258	0.2793	152.44
12	0.3967	0.1106	0.258	0.324	135.18

Table 5: Step IV, 240 MeV Solenoid Mode

	z1 [m]	z2-z1 [m]	r1 [m]	r2 [m]	J [A/mm^2]
1	-6.0063	0.1106	0.258	0.324	135.18
2	-5.8582	1.3143	0.258	0.2793	152.44
3	-4.5063	0.1106	0.258	0.3176	127.37
4	-4.1508	0.1995	0.258	0.2878	66
5	-3.7116	0.2012	0.258	0.3027	71
6	-3.06	0.21	0.263	0.347	71
7	-2.65	0.21	0.263	0.347	71
8	-1.99	0.2012	0.258	0.3027	71
9	-1.549	0.1995	0.258	0.2878	66
10	-1.1104	0.1106	0.258	0.3176	127.37
11	-0.956	1.3143	0.258	0.2793	152.44
12	0.3967	0.1106	0.258	0.324	135.18

Table 6: Step IV, Case 5 Solenoid Mode

	z1 [m]	z2-z1 [m]	r1 [m]	r2 [m]	J [A/mm^2]
1	-6.0063	0.1106	0.258	0.324	135.18
2	-5.8582	1.3143	0.258	0.2793	152.44
3	-4.5063	0.1106	0.258	0.3176	127.37
4	-4.1508	0.1995	0.258	0.2878	16
5	-3.7116	0.2012	0.258	0.3027	44
6	-3.06	0.21	0.263	0.347	113
7	-2.65	0.21	0.263	0.347	113
8	-1.99	0.2012	0.258	0.3027	44
9	-1.549	0.1995	0.258	0.2878	16
10	-1.1104	0.1106	0.258	0.3176	127.37
11	-0.956	1.3143	0.258	0.2793	152.44
12	0.3967	0.1106	0.258	0.324	135.18

A.2. Step VI

Table 7: Step VI, 200 MeV Flip Mode

	z1 [m]	z2-z1 [m]	r1 [m]	r2 [m]	J [A/mm^2]
1	-5.8957	-0.1106	0.258	0.324	135.18
2	-4.5439	-1.3143	0.258	0.2793	152.44
3	-4.3958	-0.1106	0.258	0.3176	127.37
4	-3.9513	-0.1995	0.258	0.2878	150.52
5	-3.5104	-0.2012	0.258	0.3027	142.48
6	-2.85	-0.21	0.263	0.347	136.74
7	-2.44	-0.21	0.263	0.347	-136.74
8	-1.25	-0.25	0.725	0.8356	-115.45
9	-0.1	-0.21	0.263	0.347	-136.74
10	0.1	0.21	0.263	0.347	-136.74
11	1.25	0.25	0.725	0.8356	-115.45
12	2.44	0.21	0.263	0.347	-136.74
13	2.85	0.21	0.263	0.347	136.74
14	3.5104	0.2012	0.258	0.3027	142.48
15	3.9513	0.1995	0.258	0.2878	150.52
16	4.3958	0.1106	0.258	0.3176	127.37
17	4.5439	1.3143	0.258	0.2793	152.44
18	5.8957	0.1106	0.258	0.324	135.18

Table 8: Step VI, 240 MeV Flip Mode

	z1 [m]	z2-z1 [m]	r1 [m]	r2 [m]	J [A/mm^2]
1	-5.8957	-0.1106	0.258	0.324	135.18
2	-4.5439	-1.3143	0.258	0.2793	152.44
3	-4.3958	-0.1106	0.258	0.3176	127.37
4	-3.9513	-0.1995	0.258	0.2878	137.13
5	-3.5104	-0.2012	0.258	0.3027	118.56
6	-2.85	-0.21	0.263	0.347	113.95
7	-2.44	-0.21	0.263	0.347	-113.95
8	-1.25	-0.25	0.725	0.8356	-96.21
9	-0.1	-0.21	0.263	0.347	-113.95
10	0.1	0.21	0.263	0.347	-113.95
11	1.25	0.25	0.725	0.8356	-96.21
12	2.44	0.21	0.263	0.347	-113.95
13	2.85	0.21	0.263	0.347	113.95
14	3.5104	0.2012	0.258	0.3027	118.56
15	3.9513	0.1995	0.258	0.2878	137.13
16	4.3958	0.1106	0.258	0.3176	127.37
17	4.5439	1.3143	0.258	0.2793	152.44
18	5.8957	0.1106	0.258	0.324	135.18

Table 9: Step VI, 200 MeV Solenoid Mode

	z1 [m]	z2-z1 [m]	r1 [m]	r2 [m]	J [A/mm^2]
1	-5.8957	-0.1106	0.258	0.324	135
2	-4.5439	-1.3143	0.258	0.2793	152
3	-4.3958	-0.1106	0.258	0.3176	127
4	-3.9513	-0.1995	0.258	0.2878	55
5	-3.5104	-0.2012	0.258	0.3027	62
6	-2.85	-0.21	0.263	0.347	60
7	-2.44	-0.21	0.263	0.347	60
8	-1.25	-0.25	0.725	0.8356	87
9	-0.1	-0.21	0.263	0.347	60
10	0.1	0.21	0.263	0.347	-60
11	1.25	0.25	0.725	0.8356	-87
12	2.44	0.21	0.263	0.347	-60
13	2.85	0.21	0.263	0.347	-60
14	3.5104	0.2012	0.258	0.3027	-62
15	3.9513	0.1995	0.258	0.2878	-55
16	4.3958	0.1106	0.258	0.3176	-127
17	4.5439	1.3143	0.258	0.2793	-152
18	5.8957	0.1106	0.258	0.324	-135

Table 10: Step VI, 240 MeV Solenoid Mode

	z1 [m]	z2-z1 [m]	r1 [m]	r2 [m]	J [A/mm^2]
1	-5.8957	-0.1106	0.258	0.324	135
2	-4.5439	-1.3143	0.258	0.2793	152
3	-4.3958	-0.1106	0.258	0.3176	127
4	-3.9513	-0.1995	0.258	0.2878	66
5	-3.5104	-0.2012	0.258	0.3027	71
6	-2.85	-0.21	0.263	0.347	71
7	-2.44	-0.21	0.263	0.347	71
8	-1.25	-0.25	0.725	0.8356	105
9	-0.1	-0.21	0.263	0.347	71
10	0.1	0.21	0.263	0.347	-71
11	1.25	0.25	0.725	0.8356	-105
12	2.44	0.21	0.263	0.347	-71
13	2.85	0.21	0.263	0.347	-71
14	3.5104	0.2012	0.258	0.3027	-71
15	3.9513	0.1995	0.258	0.2878	-66
16	4.3958	0.1106	0.258	0.3176	-127
17	4.5439	1.3143	0.258	0.2793	-152
18	5.8957	0.1106	0.258	0.324	-135

Table 11: Step VI, Case 5 Solenoid Mode

	z1 [m]	z2-z1 [m]	r1 [m]	r2 [m]	J [A/mm^2]
1	-5.8957	-0.1106	0.258	0.324	135
2	-4.5439	-1.3143	0.258	0.2793	152
3	-4.3958	-0.1106	0.258	0.3176	127
4	-3.9513	-0.1995	0.258	0.2878	16
5	-3.5104	-0.2012	0.258	0.3027	44
6	-2.85	-0.21	0.263	0.347	113
7	-2.44	-0.21	0.263	0.347	113
8	-1.25	-0.25	0.725	0.8356	44
9	-0.1	-0.21	0.263	0.347	113
10	0.1	0.21	0.263	0.347	-113
11	1.25	0.25	0.725	0.8356	-44
12	2.44	0.21	0.263	0.347	-113
13	2.85	0.21	0.263	0.347	-113
14	3.5104	0.2012	0.258	0.3027	-44
15	3.9513	0.1995	0.258	0.2878	-16
16	4.3958	0.1106	0.258	0.3176	-127
17	4.5439	1.3143	0.258	0.2793	-152
18	5.8957	0.1106	0.258	0.324	-135